Radiation Oncology Articles

Radiation Oncology

6-1-2022

Magnetic resonance imaging-only-based radiation treatment planning for simultaneous integrated boost of multiparametric magnetic resonance imaging-defined dominant intraprostatic lesions

Michael Dumas

Marisa Leney

Joshua Kim

Parag Sevak

Mohamed A. Elshaikh

See next page for additional authors

Authors

Michael Dumas, Marisa Leney, Joshua Kim, Parag Sevak, Mohamed A. Elshaikh, Milan Pantelic, Benjamin Movsas, Indrin J. Chetty, and Ning Wen

ORIGINAL ARTICLE

WILEY

Magnetic resonance imaging-only-based radiation treatment planning for simultaneous integrated boost of multiparametric magnetic resonance imaging-defined dominant intraprostatic lesions

Michael Dumas[1] | Marisa Leney[2] | Joshua Kim[1] | Parag Sevak[3] |
Mohamed Elshaikh[1] | Milan Pantelic[4] | Benjamin Movsas[1] | Indrin J. Chetty[1] |
Ning Wen[5] (ID)

[1]Department of Radiation Oncology, Henry Ford Health System, Detroit, Michigan, USA

[2]Northern Light Health, Brewer, Maine, USA

[3]Columbus Regional Healthcare System, Columbus, Ohio, USA

[4]Department of Radiology, Henry Ford Health System, Detroit, Michigan, USA

[5]Department of Radiology, Ruijin Hospital, Shanghai Jiao Tong University School of Medicine, Shanghai, China

Correspondence
Ning Wen, Department of Radiology, Ruijin Hospital, Shanghai Jiao Tong University School of Medicine, Shanghai, China.
Email: al2600@gmail.com

Abstract

Objective: To assess the feasibility of using synthetic computed tomography for treatment planning of the dominant intraprostatic lesion (DIL), a high-risk region of interest that offers potential for increased local tumor control.

Methods: A dosimetric study was performed on 15 prostate cancer patients with biopsy-proven prostate cancer who had undergone magnetic resonance imaging. DILs were contoured based on the turbo spin echo T2-weighted and diffusion weighted images. Air, bone, fat, and soft tissue were segmented and assigned bulk-density HU values of –1000, 285, –50, and 40, respectively, to create a synthetic computed tomography. Simultaneous integrated boost (SIB) and standard treatment plans were created for each patient. The total dose was 79.2 Gy to the non-boosted planning target volume for both plans with a boost of 100 Gy for the DIL in the SIB plan. A radiobiological model was created to determine individualized dose–response curves based on the patient's apparent diffusion coefficient maps.

Results: Mean doses to the non-boost planning target volume were 81.2 ± 0.3 Gy with the SIB and 81.0 ± 0.4 Gy without. For the DIL, the boosted mean dose was 102.6 ± 0.6 Gy. Total motor unit was 860 ± 100 with the SIB and 730 ±100 without. Femoral heads, rectum, bladder, and penile bulb were within established dose guidelines for either treatment technique. The average tumor control probability was 94% with the SIB compared with 78% without boosting the DIL.

Conclusion: This study showed the feasibility of magnetic resonance imaging-only treatment planning for patients with prostate cancer with a SIB to the DIL. DIL dose can be escalated to 100 Gy on synthetic computed tomography, while maintaining the original 79.2 Gy prescription dose and the organ of interest clinical dose limits.

1 | INTRODUCTION

Pathological studies have shown that dominant intraprostatic lesions (DIL) play an important role in prostate cancer progression, and might be considered the epicenter of local recurrence post-treatment.[1,2] Curative options for localized prostate carcinoma, including surgery and image-guided radiotherapy, have proven to be the standard of care by effectively controlling localized disease. Various clinical trials (RTOG 0126) have shown improved tumor control with escalated radiation dose to the entire prostate.[3,4] However, dose escalation increases the treatment-related normal tissue complication probability (NTCP).

Multiparametric magnetic resonance imaging (MP-MRI) is an emergent standard of care for the detection of localized prostate cancer. MP-MRI provides superior morphological and functional information by blending T2-weighted imaging and diffusion-weighted imaging (DWI). The combination of T2-weighted imaging and DWI has been shown to provide high sensitivity/specificity (performance 0.8–0.9) in DIL identification, and has been recommended in current consensus guidelines.[5,6] At the same time, the application of MRI in radiation oncology has grown. MRI offers excellent soft tissue contrast for target and organ delineation, and can track tumor motion during treatment without extra radiation exposure or treatment interruption. In addition, MRI can probe biological properties using diffusion or perfusion imaging, and assess tumor and normal tissue response during treatment. For example, apparent diffusion coefficient (ADC) maps can be correlated to clonogen cell density in the tumor. The evaluation of clonogen number changes over the treatment course can provide insights of local tumor control over time. However, MRI does not contain electron density information, which is essential for dose calculation. Multiple methods have been proposed to generate synthetic computed tomography (CT). As DIL is small, in the order of a couple milliliters, geometric uncertainty is a key consideration in synthetic CT generation.

The present study describes the development of a MRI-only workflow using synthetic CT images generated from MR images for prostate treatment planning incorporating a simultaneous integrated boost (SIB) to the MP-MRI-defined DIL, while aiming to maintain standard prescription dose to the prostate gland (79.2 Gy) and keep the normal tissue doses within established limits. The radiobiological model is used to compare the SIB approach and standard care by incorporating tumor clonogenic cell density derived from the DWI.

2 | METHODS

A retrospective dosimetric study was performed with 15 biopsy-proven prostate cancer patients that had undergone diagnostic MRI scans. An experienced radiologist delineated the prostate and DIL contours for each patient using the MP-MRI. A 5-mm margin was added to the prostate and the DIL, to create the planning target volumes (PTV$_{prostate}$ and PTV$_{DIL}$).

MR images were acquired using an Ingenia 3.0 T magnetic resonance system (Philips Medical Systems, Best, the Netherlands). Two MRI sequences were utilized to delineate the dominant intraprostatic lesions: 2-D turbo spin echo T2-weighted imaging (T$_E$/T$_R$ = 4389/110 ms, FA = 90°, voxel size = 0.42 × 0.42 × 2.4 mm^3) and DWI (T$_E$/T$_R$ = 4000/85 ms, FA = 90°, voxel size = 1.79 × 1.79 × 0.56 mm^3, with b-values = 0 and 1000 [s/mm^2]).[11] The 3-D GRE mDixon T1 image set (in-phase: T$_E$/T$_R$ = 2288/4067 ms, out-phase: T$_E$/T$_R$ = 1116/4067 ms, FA = 12°, voxel size = 0.63 × 0.63 × 1.9 mm^3) was used to create the synthetic CTs for treatment planning. For three patients, the mDixon images were rigidly registered to diagnostic CT image sets using the open-source software, Elastix (University Medical Center Utrecht, Utrecht, the Netherlands), to fill in the superficial fat tissue.[12,13] For a patient without a diagnostic CT, the peripheral tissue was determined by extrapolating the boundary regions from the mDixon images. These regions were then assigned a HU value corresponding to fat (–50 HU).

The synthetic CT generation is based on bulk density HU assignment to soft tissue, fat, bone, and air using the mDixon images. The advantage of using the mDixon technique is the ability to derive fat-only and water-only images from the in-phase and out-phase sequences, simplifying the segregation of fat and soft tissue image components. In this approach, a k-means clustering algorithm is utilized to segment soft tissue and fat.[14] This algorithm divides n objects into k clusters by assigning each object to the cluster with the nearest mean value. Segmentation of bone and air in MR images is problematic due to the relative absence of acquired signal for both structures. For this reason, the pelvic bones were manually contoured by an experienced physicist. Bulk densities were assigned to air, bone, fat, and soft tissue (–1000, 285, –50, 40 HU, respectively) as seen in Figure 1.[15]

Treatment plans were created on synthetic CTs using Eclipse treatment planning software (Varian Medical Systems, Palo Alto, CA, USA) with two 360° arcs and high-definition multileaf collimator system. Two treatment plans per patient were generated: a standard fractionation prostate plan (PTV$_{prostate}$ 79.2 Gy in 44 fractions) and a SIB plan. The SIB plan prescribed 79.2 Gy to the PTV$_{prostate}$ and 100 Gy to the PTV$_{DIL}$ in 44 fractions. This fractionation scheme is based on the focal lesion ablative microboost in prostate cancer (FLAME) clinical trial.[16] The organs at risk (OARs), including the rectum, bladder, femoral heads, and the penile bulb, were contoured on the mDixon images.

Using dose–volume histograms (DVH), D95, D99, and the maximum dose to the DIL and PTV were analyzed to assess dose coverage. The OAR constraints were based on NRG/QUANTEC protocols
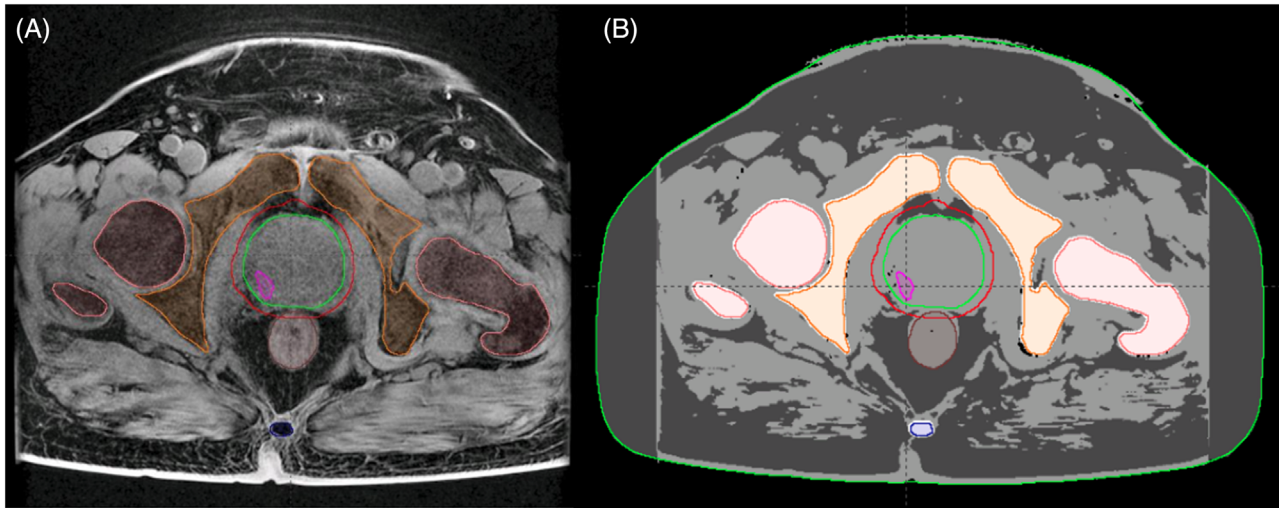
FIGURE 1   (A) mDixon magnetic resonance image and (B) synthetic computed tomography (right) with femoral (pink), pelvic (orange), and spinal bones (blue), planning target volume (red), prostate (green), dominant intraprostatic lesion (magenta), bladder (yellow), and rectum (brown)

for both plans.[17,18] Namely, V70 and V75 were analyzed for the rectum, to assess the risk of late rectal toxicity. V70 and V75 were analyzed for the bladder, where observable symptoms are the end-point. For the femoral heads, D5 was calculated due to the risk of bone necrosis. Finally, the mean dose for the penile bulb was assessed as a result of severe erectile dysfunction risk.

In addition to DVH comparisons, radiobiological modeling was used to evaluate treatment outcomes. A linear Poisson tumor control probability (TCP) formulation was created and the Lyman–Kutcher–Burman Model for NTCP was used.[19,20] All calculations were performed using BioSuite 12 (developed by Julian Uzan, NHS Clatterbridge Center for Oncology, Birkenhead, UK).

Several studies investigated the α/β ratio for prostate cancer with varying results.[21–23] TCP values were determined using $\alpha/\beta = 1.93$ Gy based on the meta-analysis of Vogelius and Bentzen.[24] A key aspect of TCP modeling is the clonogen density. ADC values are known to have a significant negative correlation with clonogen density in prostate cancer.[25] We therefore adopted a method developed by Casares-Magaz et al. to calculate clonogen density, wherein the clonogen density for the DIL was based on average ADC values inside the lesion, whereas the rest of the prostate was given a constant density of 10^5 clonogens per cm^3.[26] The patient ADC information, calculated clonogen density, and the DIL volume are tabulated in Table 1. The overall TCP for the prostate was calculated by multiplying the DIL's TCP with the TCP for the remaining volume of the prostate.

Another consideration for radiobiological modeling was tumor regrowth. This is incorporated into the linear quadratic model by the repopulation correction factor, which is calculated as $exp(ln(2) \cdot T/T_{eff})$, where T is the total treatment duration and T_{eff} is the effective doubling time of the tumor. An onset time, T_k, is also applied, as clonogen repopulation does not typically occur immediately. All TCP calculations were performed with $T_{eff} = 28$ days and $T_k = 30$ days.[26,27]

For NTCP calculations, the Lyman–Kutcher–Burman model was implemented to find the NTCP for the rectum, which is considered the most radiosensitive organ for prostate cancer treatments per QUANTEC.[17] The values for the NTCP modeling are based on the meta-analysis carried out by QUANTEC, where m (slope) is 0.13, n (volume effects) is 0.09, dose where toxicity occurs in 50% of cases (TD50) is 76.9 Gy, and α/β for the rectum is 3 Gy.[17,28] Rectal NTCP values were generated for both plans, with an end-point of grade $\geq$2 rectal bleeding.

3 | RESULTS

Table 2 lists the PTV and OAR dose statistics for each planning technique. The average PTV$_{prostate}$ D95 for the standard and SIB plans were similar at 99.1% of the prescription dose. Figure 2 shows the location of the global maximum. For the SIB plan, the average maximum dose was (105.5 ± 1.2) Gy.

All OAR doses were within QUANTEC constraints for prostate treatment. No significant difference ($p > 0.05$) was observed for the dose statistics between the standard and SIB plans. The rectal V75 was (7.5 ± 2.3)% for the standard plan and (7.2 ± 2.3)% for the SIB plan. For the bladder, the V75 was (8.9 ± 3.9)% for the standard plan and (8.6 ± 3.8)% for the SIB plan. The maximum dose for the rectum and bladder were <85 Gy for each plan. Figure 3 shows the DVHs for patient 9 as a typical example. For patient 9, the D95 for the PTV were slightly higher for the standard plan (79.4 Gy vs. 78.7 Gy for D95). The rectum and femoral heads DVH were slightly lower for the SIB over the standard plan, whereas, the bladder dose increased for SIB plan. This was due to the shallower shoulder of the PTV$_{prostate}$ DVH on the SIB plan.

Further analysis showed that patient 7 exhibited the lowest PTV and DIL D95 for the SIB plan (DIL D95 of 99.5 Gy and PTV D95 of 77.3 Gy). This patient also received the highest rectal dose, as the DIL was located in close proximity to the rectal interface. This led to a high dose to the rectum in both plans, while negatively impacting the

TABLE 1 Dominant intraprostatic lesion volume, average apparent diffusion coefficient value, and the calculated clonogen density for each patient

Patient no.	DIL volume (cm3)	Average ADC DIL (10^{-6} mm²/s)	Standard deviation	Clonogen density (10^8 /cm³)
1	1.15	1570	92	4.4
2	0.06	814	310	10.8
3	0.88	710	108	11.6
4	0.09	1118	205	8.2
5	0.04	1343	165	6.3
6	0.01	918	228	9.9
7	0.09	746	207	11.3
8	0.22	1100	206	8.4
9	0.14	704	116	11.7
10	0.11	1337	190	6.4
11	0.11	1120	189	8.2
12	0.21	1318	230	6.5
13	0.19	1016	176	9.1
14	0.16	1250	180	7.1
15	3.19	790	194	11.0

ADC, apparent diffusion coefficient; DIL, dominant intraprostatic lesion volume.

TABLE 2 Dose statistics for the standard plan and the simultaneous integrated boost plan

		Standard	SIB
PTV$_{Prostate}$	D95 (Gy)	78.5 ± 0.6	78.5 ± 0.6
	Mean Dose (Gy)	81.0 ± 0.4	81.2 ± 0.3
DIL	D95 (Gy)	80.8 ± 1.2	100.5 ± 0.5
	Mean Dose (Gy)	80.9 ± 1.2	102.6 ± 0.6
Rectum	Max. Dose (Gy)	83.8 ± 0.6	83.9 ± 0.7
	Mean Dose (Gy)	31.2 ± 5.2	30.9 ± 4.4
	V70 (%)	9.9 ± 2.8	9.8 ± 3.2
	V75 (%)	7.5 ± 2.3	7.2 ± 2.3
	NTCP (%)	6.2 ± 2.1	5.3 ± 1.7
Bladder	Max. Dose (Gy)	83.8 ± 0.8	83.7 ± 0.9
	Mean Dose (Gy)	36.2 ± 8.9	35.4 ± 7.8
	V70 (%)	11.5 ± 4.8	11.3 ± 4.7
	V75 (%)	8.9 ± 3.9	8.6 ± 3.8
Femoral heads	Max. Dose (Gy)	38.5 ± 6.3	39.3 ± 9.5
	D5 (Gy)	29.6 ± 6.1	29.6 ± 8.3
Penile bulb	Mean Dose (Gy)	7.7 ± 5.9	7.9 ± 4.9

DIL, dominant intraprostatic lesion volume; PTV, planning target volume; SIB, simultaneous integrated boost.

PTV$_{prostate}$ and PTV$_{DIL}$ dose coverage in the boost plan; however, the rectal dose was kept within the QUANTEC tolerances.

The total MU were 18% greater for the boost plans relative to the standard plans. The averages were (730 ± 100) MU for the standard plan, and (860 ± 100) MU for the SIB plan. This trend was expected due to the higher dose to PTV$_{DIL}$ and the increased multileaf collimator modulation.

The average TCP dose–response curves along with the 95% confidence intervals for the prostate and DIL are shown in Figure 4. The average TCP for the DIL was 99% at 100 Gy, compared with 83% at 79.2 Gy. The overall TCP of (94 ± 2)% for the SIB plan was a sizeable improvement relative to the non-SIB TCP of (79 ± 9)%. Lowering the average PTV$_{DIL}$ dose to 88.5 Gy would still achieve a DIL TCP of 98%.

Rectal NTCP results are tabulated in Table 2. The average rectal NTCP was 6.2% (95% CI 5.2%–7.3%) for the standard plan and 5.3% (95% CI 4.5%–6.5%) for the SIB plan. The maximum NTCP (9.8%) was observed in patient 3. This is may be caused by the higher hotspot in the PTV$_{prostate}$, allowing for less dose falloff to the rectum.

4 | DISCUSSION

Pilot studies have shown that the administration of a boost dose to the DIL increases the probability of tumor control.[29–33] Simultaneous dose escalation to the DIL without an increase in the risk of late complications has the potential to improve local tumor control for prostate cancer patients. To achieve this, it is critical to accurately delineate the DIL, boost the dose to DIL without compromising the OARs, and predict the clinical outcome in the early stages of planning. We developed an MRI-only workflow to define the DIL on MP-MRI images, delineate prostate and OARs on morphological MR images, generate synthetic CT from mDixon images for dose calculation, and generate an individualized radiobiological model incorporating clonogen
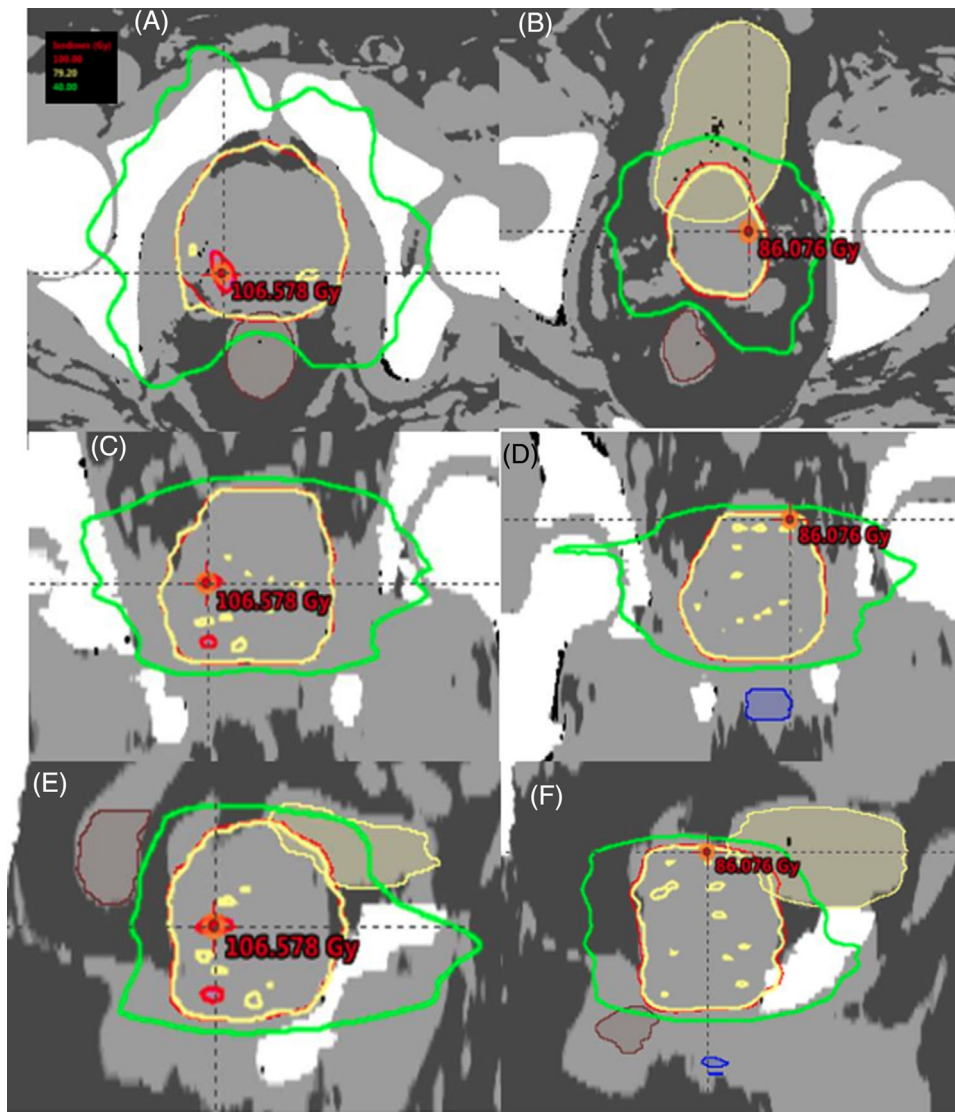
FIGURE 2 (A,B) Axial, (C,D) coronal, and (E,F) sagittal slices of the dose distribution for patient 9 (A,C,E) with and (B,D,F) without simultaneous integrated boost

density directly derived from ADC maps to assess patient therapeutic ratios.

Initial efforts to incorporate MRI in treatment planning used registration to the CT simulation image set and propagation of the MRI-derived contours to the CT images used for dose calculations. Several approaches have been proposed to improve image registration between MRI and CT in the pelvic region, including the thin-plate spline algorithm, landmark method, and biomechanical models, but an intrinsic deficiency in delineating prostate boundaries on CT images makes deformable image registration challenging.[7–10] Considering the small DIL sizes, MRI-to-CT contour propagation based on deformable image registration could introduce geometrical errors that compromise this strategy's efficacy. For these reasons, a method of prostatic radiation treatment with simultaneous boost doses to the DIL solely using MRI would be desirable.

Approaches for developing synthetic CTs from MRI include voxel-based conversion, atlas-based, and machine learning-based methods.[14,34,35,36] For voxel-based conversion, voxel values from MR images are used to calculate CT voxel values. Atlas-based synthetic CTs require a set of co-registered CT and MR images to create a set of co-registered atlases that can be deformably registered to a patient's MR images. Machine learning synthetic CTs are created based on algorithms trained from a set of MR-CT registrations. The generative adversarial network is currently the most popular machine learning algorithm. These methods may lead to geometrically accurate synthetic CTs, but some issues are present with the approaches. One issue for the voxel-based conversion method is an inability to handle the lack of consistency between voxel values across MRI scans for a specific tissue type. Sufficient variability between voxel values of a specific tissue prevents adequate optimization of assigned weights, resulting in inaccurate HU values for the synthetic CT. The use of mDixon images results in weights that are not accurate for the entire image set, rendering this method impractical for our approach. The atlas-based and generative adversarial network algorithm-based methods require
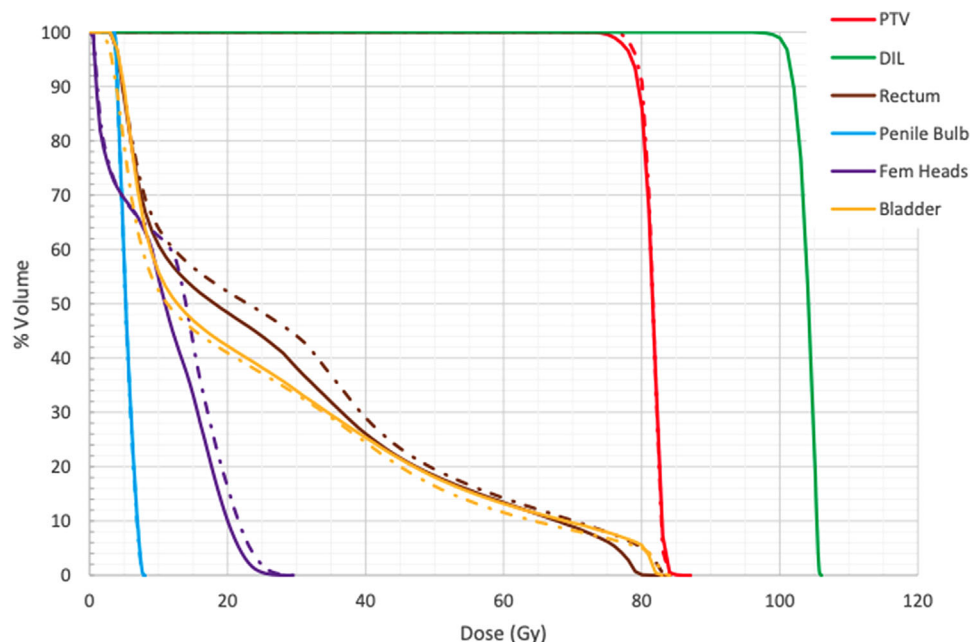
FIGURE 3 The simultaneous integrated boost (solid lines) and standard plan (dashed lines) dose–volume histograms for patient 9. DIL, dominant intraprostatic lesion; PTV, planning target volume
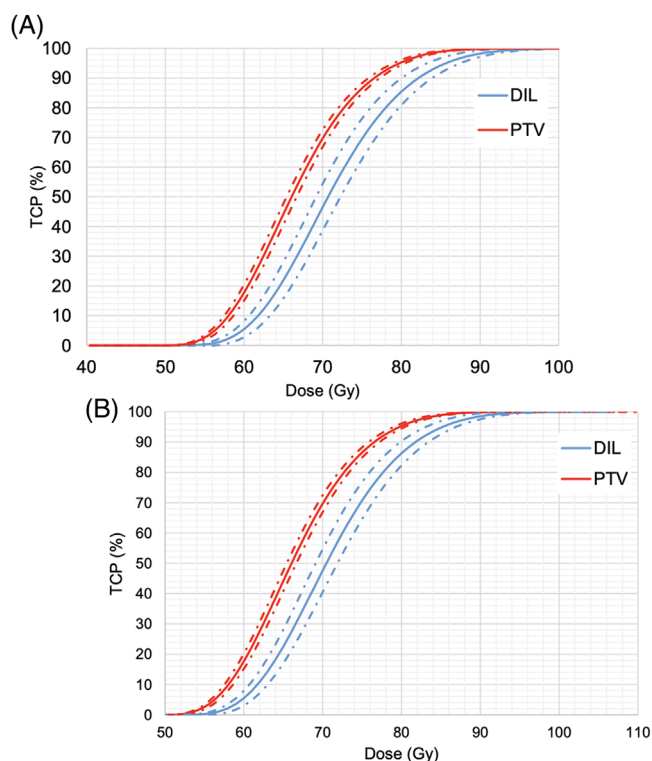

FIGURE 4 Tissue complication probability (TCP) dose–response curves for (A) the standard and (B) the simultaneous integrated boost plans. The solid line represents the mean curves and the dashed lines represent the upper and lower 95% confidence interval. DIL, dominant intraprostatic lesion; PTV, planning target volume

an extensive set of patients with both CT and MR images to generate a synthetic CT atlas or MR-CT training set.[35,36] If the set is not large enough, the models will not be able to accurately generate synthetic CTs. Another issue is registration errors between the CT-MR training set will propagate into the models, leading to inaccuracies in the synthetic CTs. This is one of the limitations of generative adversarial network-based methods, as it still needs perfectly registered MRI and CT training pairs for image synthesis, which is difficult to achieve in the pelvic region with large organ deformations. Additionally, several studies have investigated the dosimetric accuracy of bulk density assigned synthetic CTs. They showed a dose uncertainty of <1.5%.[15,37,38] For this reason, it was determined that bulk density synthetic CTs, while not as accurate as the voxel-based conversion or atlas-based methods, were the most viable option for treatment planning. Although we noted that our reported method incorporated CT images to fill in the excluded periphery of the acquired mDixon images in three patients, a future adjustment to the MRI protocol to include skin-to-skin coverage of all patients would mitigate this step and allow a complete MRI-only workflow with more accurate synthetic CTs.

With respect to TCP, the best DIL result for the standard plan was for patient 6, with 96% TCP due to a small lesion size. Patient 6's PTV$_{DIL}$ was 1.37 cm^3, the smallest treatment volume of the patient cohort. A small lesion can result in high TCP, even without boosting the dose. This implies that although clonogen density plays a role, TCP also depends on the lesion volume. Small lesions can be controlled more easily, independent of clonogen density; however, the correlation between the lesion size and clonogen density is complicated and requires further investigation. Patient 1 had a larger lesion (1.15 cm^3) than patient 3 (0.88 cm^3), but did not experience lower TCP due to clonogen density (75% TCP vs. 67% TCP for the standard plan).

Currently, there is not a consensus on the T_{eff} and T_k values in the TCP modeling for prostate cancer. Previous studies have shown variability in T_{eff} values: from as little as 0 days to 62 days.[26,39–42] These studies have shown that T_{eff} is dependent on the cancer type and staging, and could potentially be different for individual cells of the same cancer type. It is possible that T_{eff} is unique for each individual, necessitating the calculation of T_{eff} for every patient.[43] Further investigation into T_{eff} for prostate cancer is warranted, but for the present study, the value of 28 days was deemed accurate for 'medium' proliferation. For T_k values, there is less variability among published data, where the typical value is approximately 28–34 days.[21,27,40] The chosen T_k of 30 days serves as a reasonable value for biopsy-proven prostate cancer (stage T1c).[27] Some studies have incorporated immediate onset time ($T_k = 0$); however, this is not considered accurate and would result in low TCP values.[21]

We observed no significant difference in the rectal V70 and V75 between the standard and SIB plans. The rectal NTCP results showed significance, but followed the same trend as the rectum DVH. This result is unexpected with the presence of the boost dose. However, this could be produced by slight differences in plan optimization that do not show significance in the plan statistics, but nevertheless, affect the NTCP. In addition, DILs more commonly occur in the peripheral zone, often near the rectal interface, resulting in a high dose to the rectum.[44–46] Considering the present rectum DVH and NTCP results, we showed that it is possible to produce clinically acceptable MRI-only based treatment plans by boosting the dose to DIL, while maintaining prescription dose coverage to the PTV and dose constraints to rectum.

5 | CONCLUSION

We have shown a feasible implementation of MRI-only treatment planning for prostate cancer with a SIB for DIL. The dose to the DIL can be escalated to 100 Gy on the synthetic CTs, while maintaining the original prescription of 79.2 Gy and remaining within clinical criteria for the OARs. The boost dose can be lowered to approximately 90 Gy and maintain high TCP based on the generated dose response curves. Although the rectal NTCP shown differences between the SIB and standard plan, this is not considered clinically significant. Further investigation into the creation and optimization of the synthetic CT and margin for the DIL structure is warranted. If promising results are achieved, a prospective study will be implemented.

CONFLICT OF INTERESTS

No conflict of interest has been declared by the author(s).

ORCID

Ning Wen https://orcid.org/0000-0001-9776-8056

REFERENCES

1. Mouraviev V, Villers A, Bostwick DG, Wheeler TM, Montironi R, Polascik TJ. Understanding the pathological features of focality, grade and tumour volume of early-stage prostate cancer as a foundation for parenchyma-sparing prostate cancer therapies: active surveillance and focal targeted therapy. *BJU Int.* 2011;108(7):1074-1085.
2. Pucar D, Hricak H, Shukla-Dave A, et al. Clinically significant prostate cancer local recurrence after radiation therapy occurs at the site of primary tumor: magnetic resonance imaging and step-section pathology evidence. *Int J Radiat Oncol Biol Phys.* 2007;69(1):62-69.
3. Dearnaley DP, Sydes MR, Graham JD, et al. Escalated-dose versus standard-dose conformal radiotherapy in prostate cancer: first results from the MRC RT01 randomised controlled trial. *Lancet Oncol.* 2007;8(6):475-487.
4. Zietman AL, DeSilvio ML, Slater JD, et al, . Comparison of Conventional-Dose vs High-Dose Conformal Radiation Therapy in Clinically Localized Adenocarcinoma of the Prostate. *JAMA.* 2005;294:(10):1233-1239.
5. Barentsz JO, Richenberg J, Clements R, et al. ESUR prostate MR guidelines 2012. *Eur Radiol.* 2012;22(4):746-757.
6. Dickinson L, Ahmed HU, Allen C, et al. Scoring systems used for the interpretation and reporting of multiparametric MRI for prostate cancer detection, localization, and characterization: could standardization lead to improved utilization of imaging within the diagnostic pathway? *J Magn Reson Imaging.* 2013;37(1):48-58.
7. Rasch C, Barillot I, Remeijer P, Touw A, van Herk M, Lebesque JV. Definition of the prostate in CT and MRI: a multi-observer study. *Int J Radiat Oncol Biol Phys.* 1999;43(1):57-66.
8. Zhong H, Kim JP, Chetty IJ. Analysis of deformable image registration accuracy using computational modeling. *Med Phys.* 2010;37(3):970-979.
9. Zhong H, Wen N, Gordon JJ, Elshaikh MA, Movsas B, Chetty IJ. An adaptive MR-CT registration method for MRI-guided prostate cancer radiotherapy. *Phys Med Biol.* 2015;60(7):2837-2851.
10. Li S, Glide-Hurst C, Lu M, et al. Voxel-based statistical analysis of uncertainties associated with deformable image registration. *Phys Med Biol.* 2013;58(18):6481-6494.
11. Bagher-Ebadian H, Janic B, Liu C, et al. Detection of dominant intraprostatic lesions in patients with prostate cancer using an artificial neural network and MR multimodal radiomics analysis. *Front Oncol.* 2019;9:1313.
12. Klein S, Staring M, Murphy K, Viergever MA, Pluim JP. Elastix: a toolbox for intensity-based medical image registration. *IEEE Trans Med Imaging.* 2010;29(1):196-205.
13. Shamonin DP, Bron EE, Lelieveldt BP, Smits M, Klein S, Staring M. Fast parallel image registration on CPU and GPU for diagnostic classification of Alzheimer's disease. *Front Neuroinform.* 2014;7:50.
14. Kim J, Glide-Hurst C, Doemer A, Wen N, Movsas B, Chetty IJ. Implementation of a novel algorithm for generating synthetic CT images from magnetic resonance imaging data sets for prostate cancer radiation therapy. *Int J Radiat Oncol Biol Phys.* 2015;91(1):39-47.
15. Kim JP, Garbarino K, Schultz L, et al. Dosimetric evaluation of synthetic CT relative to bulk density assignment-based magnetic resonance-only approaches for prostate radiotherapy. *Radiat Oncol.* 2015;10:239.
16. Monninkhof EM, van Loon JWL, van Vulpen M, et al: Standard whole prostate gland radiotherapy with and without lesion boost in prostate cancer: Toxicity in the FLAME randomized controlled trial. *Radiother Oncol.* 2018;127(1):74-80
17. Bentzen SM, Constine LS, Deasy JO, et al. Quantitative analyses of normal tissue effects in the clinic (QUANTEC): an introduction to the scientific issues. *Int J Radiat Oncol Biol Phys.* 2010;76(3 suppl):S3-S9.
18. Lee WR et al. RTOG 0415: A phase III randomized study of hypofractionated 3D-CRT/IMRT versus conventionally fractionated 3D-CRT/IMRT in patients with favorable risk prostate cancer. 2008.
19. Allen Li X, Alber M, Deasy JO et al. The use and QA of biologically related models for treatment planning: Short report of the TG-166 of the therapy physics committee of the AAPM. *Med Phys.* 2012;39(3):1386-1409.

20. Burman C, Kutcher G, Emami B, Goitein M. Fitting of normal tissue tolerance data to an analytic function. *Int J Radiat Oncol Biol Phys.* 1991;21(1):123-135.

21. Wang JZ, Guerrero M, Li XA. How low is the α/β ratio for prostate cancer? *Int J Radiat Oncol Biol Phys.* 2003;55(1):194-203.

22. Fowler J, Chappell R, Ritter M. Is α/β for prostate tumors really low? *Int J Radiat Oncol Biol Phys.* 2001;50(4):1021-1031.

23. Hanks G, Martz K, Diamond J. The effect of dose on local control of prostate cancer. *Int J Radiat Oncol Biol Phys.* 1988;15(6):1299-1305.

24. Vogelius IR, Bentzen SM. Meta-analysis of the alpha/beta ratio for prostate cancer in the presence of an overall time factor: bad news, good news, or no news? *Int J Radiat Oncol Biol Phys.* 2013;85(1):89-94.

25. Glazer DI, Hassanzadeh E, Fedorov A, et al. Diffusion-weighted endorectal MR imaging at 3T for prostate cancer: correlation with tumor cell density and percentage Gleason pattern on whole mount pathology. *Abdom Radiol.* 2017;42(3):918-925.

26. Casares-Magaz O, Van der Heide UA, Rørvik J, Steenbergen P, Muren LP. A tumour control probability model for radiotherapy of prostate cancer using magnetic resonance imaging-based apparent diffusion coefficient maps. *Radiother Oncol.* 2016;119(1):111-116.

27. Gao M, Mayr NA, Huang Z, Zhang H, Wang JZ. When tumor repopulation starts? The onset time of prostate cancer during radiation therapy. *Acta Oncologica.* 2010;49(8):1269-1275.

28. Emami B, Lyman J, Brown A, et al. Tolerance of normal tissue to therapeutic irradiation. *Int J Radiat Oncol Biol Phys.* 1991;21(1):109-122.

29. Nutting CM, Corbishley CM, Sanchez-Nieto B, Cosgrove VP, Webb S, Dearnaley DP. Potential improvements in the therapeutic ratio of prostate cancer irradiation: dose escalation of pathologically identified tumour nodules using intensity modulated radiotherapy. *Br J Radiol.* 2002;75(890):151-161.

30. Bauman G, Haider M, Van der Heide UA, Menard C. Boosting imaging defined dominant prostatic tumors: A systematic review. *Radiother Oncol.* 2013;107(3):274-281.

31. Schild MH, Schild SE, Wong WW, et al. A prospective trial of intensity modulated radiation therapy (IMRT) incorporating a simultaneous integrated boost for prostate cancer: long-term outcomes compared with standard image guided IMRT. *Int J Radiat Oncol Biol Phys.* 2017;97(5):1021-1025.

32. Schild MH, Schild SE, Wong WW, et al. Early outcome of prostate intensity modulated radiation therapy (IMRT) incorporating a simultaneous intra-prostatic MRI directed boost. *OMICS J Radiol.* 2014;3(4):170.

33. Murray LJ, Lilley J, Thompson CM, et al. Prostate stereotactic ablative radiation therapy using volumetric modulated arc therapy to dominant intraprostatic lesions. *Int J Radiat Oncol Biol Phys.* 2014;89(2):406-415.

34. Dowling JA, Lambert J, Parker J, et al. An atlas-based electron density mapping method for magnetic resonance imaging (MRI)-alone treatment planning and adaptive MRI-based prostate radiation therapy. *Int J Radiat Oncol Biol Phys.* 2012;83(1):e5-e11.

35. Kraus KM, Jäkel O, Niebuhr NI, Pfaffenberger A. Generation of synthetic CT data using patient specific daily MR image data and image registration. *Phys Med Bio.* 2017;62(4):1358-1377.

36. Lui L, Lei Y, Wang Y, et al. Evaluation of a deep learning-based pelvic synthetic CT generation technique for MRI-based prostate proton treatment planning. *Phys Med Biol.* 2019; 64:205022.

37. Chin AL, Lin A, Anamalayil S, Teo BKK. Feasibility and limitations of bulk density assignment in MRI for head and neck IMRT treatment planning. *J Appl Clin Med Phys.* 2014;15(5):4851.

38. Lambert J, Greer PB, Menk F, et al. MRI-guided prostate radiation therapy planning: investigation of dosimetric accuracy of MRI-based dose planning. *Radiother Oncol.* 2011;98(3):330-334.

39. Haustermans KM, Hofland I, Van Poppel H, et al. Cell kinetic measurements in prostate cancer. *Int J Radiat Oncol Biol Phys.* 1997;37(5):1067-1070.

40. Withers H, Taylor J, Maciejewski B. The hazard of accelerated tumor clonogen repopulation during radiotherapy. *Acta Oncol.* 1988;27(2):131-146.

41. Lai P, Pilepich M, Krall J, et al. The effect of overall treatment time on the outcome of definitive radiotherapy for localized prostate carcinoma: the Radiation Therapy Oncology Group 75-06 and 77-06 experience. *Int J Radiat Oncol Biol Phys.* 1991;21(4):925-933.

42. Perez CA, Michalski J, Mansur D, Lockett MA. Impact of elapsed treatment time on outcome of external-beam radiation therapy for localized carcinoma of the prostate. *Cancer J.* 2004;10(6):349-356.

43. Fowler JF, Ritter MA. A rationale for fractionation for slowly proliferating tumors such as prostatic adenocarcinoma. *Int J Radiat Oncol Biol Phys.* 1995;32(2):521-529.

44. De Meerleer G, Villeirs G, Bral S, et al. The magnetic resonance detected intraprostatic lesion in prostate cancer: planning and delivery of intensity-modulated radiotherapy. *Radiother Oncol.* 2005;75(3):325-333.

45. Rosenkrantz AB, Deng F-M, Kim S, et al. Prostate cancer: multiparametric MRI for index lesion localization—a multiple-reader study. *AJR Am J Roentgenol.* 2012;199(4):830-837.

46. Russo F, Regge D, Armando E, et al. Detection of prostate cancer index lesions with multiparametric magnetic resonance imaging (mp-MRI) using whole-mount histological sections as the reference standard. *BJU Int.* 2016;118(1):84-94.